Journal Pre-proof

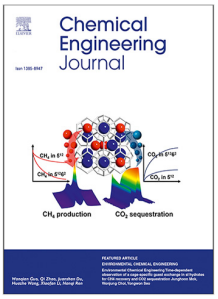

Mitigating the capacity loss by crossover transport in vanadium redox flow battery: A chemometric efficient strategy proposed using finite element method simulation

Luis Felipe Pilonetto, Felipe Staciaki, Eryka Nóbrega, Evaldo B. Carneiro-Neto, Jeyse da Silva, Ernesto Pereira

PII: S1385-8947(23)04067-6
DOI: https://doi.org/10.1016/j.cej.2023.145336
Reference: CEJ 145336

To appear in: *Chemical Engineering Journal*

Received date : 31 May 2023
Revised date : 4 August 2023
Accepted date : 8 August 2023

Please cite this article as: L.F. Pilonetto, F. Staciaki, E. Nóbrega et al., Mitigating the capacity loss by crossover transport in vanadium redox flow battery: A chemometric efficient strategy proposed using finite element method simulation, *Chemical Engineering Journal* (2023), doi: https://doi.org/10.1016/j.cej.2023.145336.

Mitigating the capacity loss by crossover transport in vanadium redox flow battery: A chemometric eficient strategy proposed using finite element method simulation

Luis Felipe Pilonetto[a], Felipe Staciaki[a], Eryka Nóbrega[a], Evaldo B. Carneiro-Neto, Jeyse da Silva[a], Ernesto Pereira[a,*]

[a]Chemistry Department, Federal University of São Carlos, 13565-905, São Carlos, SP, Brazil

Abstract

Energy storage systems play a major role in the energy transition. Among them, vanadium redox flow batteries are a promising alternative to conventional batteries, which due to their design can be scaled, and it is possible to decouple power and energy density. However, the transport of electroactive species through the membrane (cross-contamination) reduces the capacity and useful life of these batteries. In this work, computational simulation was performed using the finite element method coupled to chemometric analysis to develop a mitigation strategy to decrease the vanadium redox flow batteries capacity loss by cross-contamination. This study can be divided into two stages. Initially, a 2^3 full factorial design was performed to evaluate and determine the effect of different variables: current density, active species concentration, and volumetric flow on the loss of capacity of vanadium redox flow batteries. In the second stage, a Doehlert design was performed with current density, the concentration of active species, and the volumetric flow between electrolyte tanks as variables to obtain the optimum conditions that minimize capacity loss. The results show that the current density and the concentration of active species are the main variables that affect capacity loss in vanadium redox flow batteries. The

*Corresponding author
Email address: ernesto@ufscar.br (Ernesto Pereira)
Preprint submitted to Elsevier

August 4, 2023

proposed approach successfully mitigated the cross-contamination in different combinations of current density and concentration of active species providing an optimal flow between electrolyte tanks for different operating conditions.

Keywords: flow batteries, CFD simulation, chemometric analysis, VRFB capacity loss.

Nomenclature

Abbreviations

ESSs	Energy Storage Systems
FEM	Finite Element Method
RFB	Redox Flow Battery
VRFB	Vanadium Redox Flow Battery

Symbols

$(\mu)^{e,j}$	Dynamic viscosity of the electrolyte
ϵ	Porosity of electrode
η	Overpotential
κ	Permeability of electrode
i_l	Electrolyte current density
i_s	Electrode current density
N_i	Flux of chemical species
v	Flow velocity
ω	Volumetric flow

34	ω_{br}	Volumetric flow between reservoirs
35	φ_s	Electrode potential
36	σ_s^{eff}	Effective conductivity of porous electrode
37	a_a	Anodic charge transfer coefficient
38	a_c	Cathodic charge transfer coefficient
39	C_d	Discharging capacity
40	C_d^{th}	Capacity at n^{th} cycle
41	c_{act}	Active species concentration
42	$c_{i,0}$	Initial concentration of the species i
43	c_{sup}	Supporting electrolyte concentration
44	CL	Capacity loss
45	CL_{rate}	Capacity loss rate
46	D_i	Diffusion coefficient
47	D_i^{eff}	Effective diffusion coefficient
48	E^0	Standard potential (V)
49	H	Cell height
50	i_0	Exchange current density
51	i_{loc}	Local current density
52	j	Current density
53	n_i^r	Quantity of i species in electrolyte reservoirs

n_{cycles}	Number of cycles
p	Pressure
SoC	State of charge
T	Temperature
$t_{d,n^{th}}$	Discharge time of the first cycle
$t_{d,n^{th}}$	Discharge time of the n^{th} cycle
v	Linear velocity inside the cell
$V^{t,j}$	Volume of reservoir
V_0	Initial volume of reservoir
W_{cell}	Cell width

Physical Constants

R	Ideal gas constant 8.314 J K^{-1} mol^{-1}
F	Faraday's constant 96485 C mol^{-1}

1. Introduction

The energy demand has sharply increased worldwide recently, and it is expected to keep rising annually. In order to meet global energy demand, conventional non-renewable energy sources (such as coal, oil, and gas) have been employed, which has resulted in an energy crisis and difficulties with environmental pollution. [1]

In order to address the aforementioned challenges, the imperative shift toward a carbon-neutral economy is a pivotal transformation. However, renewable power generation, such as solar and wind, has the characteristics of randomness

and intermittence. [2, 3] For this reason, the wide application of this type of energy source is highly dependent on energy storage systems (ESSs). One way to overcome such difficulties is the development of energy storage technologies that allow its continuous use. [4] Storage also provides flexibility in the control and maintenance of the power grid, allowing energy to be supplied on demand. [5]

Batteries are one of the main systems used to store electrical energy due to their advantages over other systems. An example is the versatility that these systems have, as they can be installed anywhere, free from geological restrictions. [6] However, for application in large-scale networks, storage batteries must have a high number of charge/discharge cycles, a long service life, high efficiency, and adequate production and maintenance costs. [7, 8]

The most commercially used batteries are lithium-ion batteries, which have long life cycles and high efficiency, [6] but with high production costs due to limited lithium reserves. [9, 10] In this context, redox flow batteries (RFBs) are a promising alternative to meet the aforementioned requirements. [11] They offer low production cost, flexibility, mobility, fast response, simple design, and the ability to support a floating power supply. In addition, they present safety advantages over the most used batteries. [11–13] Such technology, although commercially viable, is at the limit of its development. For this reason, to optimize the performance of flow batteries, new proposals must be considered.

Historically, a series of flux batteries began to be reported, including batteries free of ion exchange membranes, such as lead-acid, [14] zinc-nickel [15] and zinc-cerium, [16] which have greater simplicity and lower cost compared to other RFBs. [14] Among the large number of redox flow batteries reported in the literature, semi-solid RFBs [17] composed of lithium pairs[18, 19] in suspension are also found. These batteries have lower costs compared to conventional

lithium-ion batteries. [20]

However, all batteries mentioned above are subject to the cross-contamination effect, which led to the development of mixed electrolytes for RFBs. [21] In this context, vanadium-only redox pair batteries (VRFBs) [22] have also emerged, which are in an advanced stage of development and are already commercial. [23] Cross-contamination also occurs in VRFBs, but the products of the reactions that occur between the two half-cells are vanadium species. Thus, the capacity loss is reversible and can be mitigated by rebalancing the concentration of species consumed in the self-discharge reactions. [24]

In this sense, operational conditions are highly relevant for mitigating capacity loss in VRFBs. Wang et al. [25] proposed a volume transfer between the electrolyte reservoirs in the opposite direction to the net cross-contamination (from positive to negative electrolyte reservoir). Their results showed that capacity loss can be significantly reduced by this method. The authors also found that the VRFB current density has an interaction effect with the electrolyte transference between reservoirs. In other words, the optimal volumetric flow rate between electrolyte reservoirs that reduce capacity loss in the VRFB depends on the battery's current density. Therefore, this mitigation strategy can be improved by finding which operating conditions affect capacity loss and what should be the optimal volumetric flow between the reservoirs to minimize capacity loss taking into account the effects of these operating conditions. [25]

Traditionally, the methodologies are based on the "one variable at a time" (OVAT) approach. This procedure is simple but extremely laborious and time-consuming. As a univariate approach, it is unable to detect interactions between the variables, i.e., the effect of the value of variable A on the change of the values of variable B, as a result, it frequently produces results that are difficult to interpret, especially as the number of parameters increases. Additionally, the

OVAT approach tends to locate only local optima and may thus overlook the truly optimal parameters. [26] This continues to be an essential yet challenging, and often limiting step in the optimization process. Clearly, due to the large number of variables that control the response, their exploration using inappropriate tools is likely to generate sub-optimal solutions. In this sense, statistical tools such as Design of Experiments (DoE) make it possible to explore complex problems with minimum resources. [27, 28] DoE provides a more detailed picture of the behavior of a particular process, determines the contribution of each factor to the system, resolves their interactions, and models the effect on the response (or multiple responses). By performing just a few experiments we can generate a statistical model and effectively map and visualize the entire space of responses.

In recent years, computer simulations have increasingly proven to be useful and robust tools for studying various systems in the fields of basic sciences and engineering. Analytical solutions are typically limited to simpler systems, making it impossible to obtain an analytical solution for differential equations in complex systems. The finite element method involves numerically solving these equations and providing an approximate solution. This method allows for the simulation of complex systems with different physical phenomena. It enables the study of various electrochemical systems, including electrodeposition, corrosion, batteries, and supercapacitors. [29]

Considering the great impact that cross-contamination has on the operational life of the VRFB, in this work, the computational simulation performed by the finite element method combined with chemometric analysis has been used to evaluate the effect of operating conditions on VRFB capacity loss and to find the optimum flow between reservoirs to reduce these losses.

2. Model description and simulation procedure

The model consists of a 2D projection of a VRFB containing two electrolyte reservoirs, two current collectors, pipes, and two porous carbon felt separated by a Nafion™ membrane (Figure 1). The electrolyte reservoirs and current collectors are not present in the 2D domain and were simulated by boundary conditions. Pipes are also not present and were simulated using equations to describe the pressure loss. The model is formed by three domains: a positive electrode, a negative electrode, and an ion exchange membrane.

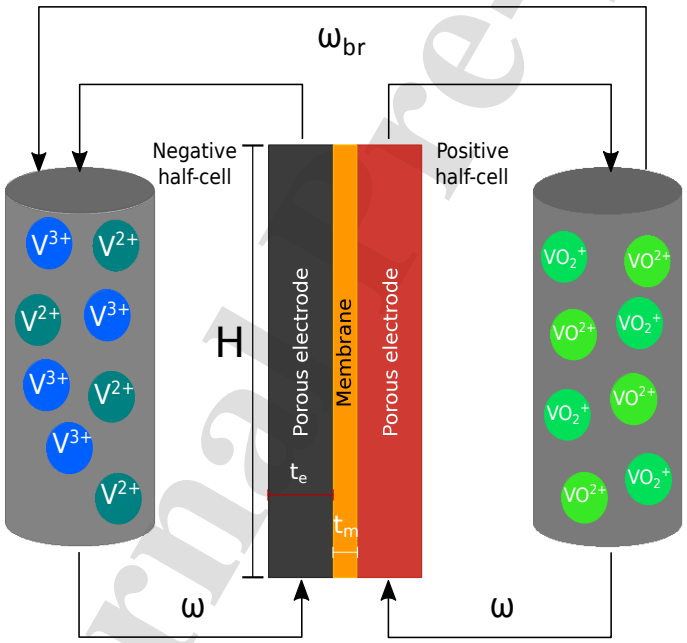

Figure 1: Schematic representation of the VRFB model.

Each electrode is fed with an electrolyte containing a vanadium redox couple and sulfuric acid. The negative electrolyte consists of aqueous solutions of sulfate salts of V^{2+} and V^{3+} and H_2SO_4. The positive electrolyte is composed

Table 1: Dimensional and operational parameters of the VRFB model

Parameter	Description	Value
h	Cell height	100 mm
t_e	Electrode thickness	4.0 mm
t_m	Membrane thickness	0.18 mm
ω	Volumetric flow	*
ω_{br}	Volumetric flow between reservoirs	*

*Values defined in the factorial design.

of dissolved VO^{2+} and VO^{3+} sulfates and H_2SO_4.

The mass conservation for each species present in the system is given by

$$\frac{\partial \epsilon c_i^e}{\partial t} + \nabla \cdot \mathbf{N}_i = -S_i \qquad (1)$$

where ϵ is the porosity of the electrode, c_i^e is the concentration for each species, N_i is the flux and S_i is the source term. The flux was calculated by the Nernst-Planck equation

$$\mathbf{N_i} = -D_i^{eff} \nabla c_i^e - z_i \upsilon_i^e c_i^e F \nabla \phi_l^e + \mathbf{v} c_i^e \qquad (2)$$

where φ_l^e is the electrolyte potential, υ_i^e is the ionic mobility, z_i is the charge of the species, v and F is Faraday's constant.

The transport of ionic species due to the electrochemical reactions and the electronic current is coupled by charge conservation as follows

$$\nabla \cdot \mathbf{i_l} + \nabla \cdot \mathbf{i_s} = 0 \qquad (3)$$

where i_l is the current density of the electrolyte and i_s is the current density of the electrode. The electronic current (i_l) is described by Ohm's law and the ionic current (i_s) by Faraday's law as follows

$$\mathbf{i_s} = \sigma_s^{eff} \nabla \phi_s \qquad (4)$$

$$\mathbf{i_l} = F \sum_i z_i \mathbf{N_i} \qquad (5)$$

where σ_s^{eff} is the effective conductivity of the porous electrode, obtained by Bruggemann correction, and φ_s is the electrode potential.

The local currents of electrochemical reactions (i_{loc}^n and i_{loc}^p) were modeled with the Butler-Volmer equation as follows

$$i_{loc}^n = aFk^n (c_{V^{2+}}^b)^{(1-\alpha^n)} (c_{V^{3+}}^b)^{\alpha^n} \left[\frac{c_{V^{2+}}^s}{c_{V^{2+}}^b} exp(\frac{(1-\alpha^n)F\eta^n}{RT} - \frac{c_{V^{3+}}^s}{c_{V^{3+}}^b} exp\left(\frac{-\alpha^n F\eta^n}{RT}\right)\right] \qquad (6)$$

$$i_{loc}^p = aFk^n (c_{VO^{2+}}^b)^{(1-\alpha^p)} (c_{VO_2^+}^b)^{\alpha^p} \left[\frac{c_{VO^{2+}}^s}{c_{VO^{2+}}^b} exp(\frac{(1-\alpha^p)F\eta^p}{RT} - \frac{c_{VO_2+}^s}{c_{VO_2+}^b} exp\left(\frac{-\alpha^p F\eta^p}{RT}\right)\right] \qquad (7)$$

where k is the rate constant, a is the specific surface area, α is the charge transfer coefficient, η is the overpotential, s is the surface concentration and b is the bulk concentration (n and p indices refer to the negative and positive half-cells, respectively)

The velocity (v) from Eq. 2 is determined by Darcy's law

$$\mathbf{v} = -\frac{\kappa}{\mu^{e,j}} \nabla \rho \qquad (8)$$

where $\mu^{e,j}$ is the dynamic viscosity of the electrolyte, p is the pressure and κ is the permeability of the electrode. The transport of vanadium species through

the membranes was considered.

The variation of species concentration in the electrolyte reservoirs was modeled by the following ODE

$$\frac{dn_i^r}{dt} = \epsilon W_{cell}\left(\int_0^{L_{out}} c_i v\, dx - \int_0^{L_{in}} c_i v\, dx\right), n_i^t(0) = c_{i,0}V_0 \qquad (9)$$

where n_i^t is the number of mols of species i in the electrolyte reservoirs, ϵ electrode porosity, W_{cell} is the cell width, v is the linear velocity inside the cell, $c_{i,0}$ is the initial concentration of the species i, V_0^t is the initial volume of the reservoir, L_{in} is the inlet electrode thickness and L_{out} is outlet electrode thickness. Considering that there is an electrolyte transfer between the half-cells due to convection across the membrane, the volume of electrolytes in each reservoir will change. This variation is given by the following equation

$$\frac{dV^{t,j}}{dt} = j\epsilon w_{cell} H v, V^{t,j}(0) = V_0^t \qquad (10)$$

where $V^{t,j}$ is the volume of each tank, W_{cell} is the cell width and j is the unit value of semi-cell representation (-1 for negative electrolyte and +1 for positive electrolyte).

To simulate the electrolyte transfer between reservoirs it is necessary to modify equation 9. Considering that the number of species in each tank depends on the flux of species between reservoirs, for VO_2^+, VO^{2+}, $VO_{neg}{}^{2+}$ and $VO_{neg}{}^+$ the equation becomes

$$\frac{dn_i^t}{dt} = \epsilon w_{cell}\left(\int_0^{L_{out}} c_i v\, dx - \int_0^{L_{in}} c_i v\, dx\right) - j\omega_{br} c_i^t \qquad (11)$$

where ω_{br} is the volumetric flow between the reservoirs. The reservoir volume becomes

$$\frac{dV^{t,j}}{dt} = \epsilon w_{cell} H v_{m,x} - j\omega_{br} \quad (12)$$

The set of differential equations was solved by the finite element method using the software COMSOL Multiphysics on a computer with a 3.5 GHz processor i7 and 131 GB of RAM. The computational simulation time was 12 hours.

2.1. Chemometric study

A 2^3 full factorial design was carried out to determine the effect of current density (j), active species concentration (c_{act}), and volumetric flow (ω) on capacity loss per cycle (CL).

The discharging capacity (C_d) is determined by

$$C_d = \frac{t_{d,n^{th}}}{t_{d,1^{st}}} \times 100\% \quad (13)$$

where $t_{d,n^{th}}$ and $t_{d,1^{st}}$ are the discharge times of the n^{th} and first cycle, respectively. Thus, CL is calculated as follows

$$CL = |100\% - C_d^{th}| \quad (14)$$

where C_d^{th} is the capacity at the n^{th} cycle.

The cut-off potential for each experiment was determined by state of charge (SoC) cut-off of 0.9 and 0.1 for the first cycle for charging and discharging procedures, respectively. The supporting electrolyte concentration was 3.0 mol L^{-1} and the capacity loss rate (CL_{rate}) was determined by

$$CL_{rate} = \sum_{1}^{i} \frac{dC_{d,i}}{dt} \frac{1}{n_{cycles}} \quad (15)$$

where n_{cycles} is the total number of cycles.

The influence of c_{act} on the viscosity in each half-cell and associated capacity loss rate was also investigated. To determine the suitable viscosity for both negative and positive electrolytes, a regression model analysis was performed with data available in the literature for the SoC, supporting electrolyte concentration (c_{sup}) and c_{act}. The viscosity parameters set up for factorial design experiments were the mean values of viscosity in each SoC. The responses (positive and negative viscosity) were individually submitted to a quadratic regression for coefficients estimation:

$$\begin{aligned}\mu^{j} = {} & \mathbf{w_0} + \mathbf{w_{01}}SoC + \mathbf{w_{02}}c_{act} + \mathbf{w_{03}}c_{sup} + \mathbf{w_{04}}T \\ & + \mathbf{w_{11}}(SoC)^2 + \mathbf{w_{12}}SoCc_{act} + \mathbf{w_{13}}SoCc_{sup} \\ & + \mathbf{w_{14}}SoCT + \mathbf{w_{22}}c_{act}^2 + \mathbf{w_{23}}c_{act}c_{sup} + \mathbf{w_{24}}c_{act}T \\ & + \mathbf{w_{33}}c_{sup}^2 + \mathbf{w_{34}}c_{sup} + \mathbf{w_{44}}T^2\end{aligned} \tag{16}$$

where T is the electrolyte temperature.

K-fold cross-validation was used to validate the performance of the model. The data set was split into five sections.

After determining the statistically significant factors, a regression model was performed for the volumetric flow between electrolyte reservoirs, to evaluate discharge capacity behavior. The optimum operating conditions are attained by using three variables in a Doehlert design: volumetric flow between reservoirs (ω_{br}), current density (j), and (c_{act}). The C L was submitted to a quadratic regression for coefficients estimation:

$$\mathbf{CL} = \mathbf{w_0} + \mathbf{w_{01}}\omega_b r + \mathbf{w_{02}} j + \mathbf{w_{03}} c_{act} + \mathbf{w_{11}}(\omega_{br})^2 + \mathbf{w_{12}}\omega_{br} j + \mathbf{w_{13}}\omega_{br} c_{act} + \mathbf{w_{22}} j^2 + \mathbf{w_{23}} j c_{act} + \mathbf{w_{33}} c_{act}^2 \quad (17)$$

According to the magnitude test presented in the Supplementary Information, ω_{br} must be of the order of 10^{-5} to minimize VRFBs capacity loss. Therefore, ω_{br} value was calculated by the following equation

$$\omega_{br} = \upsilon_p \omega 10^{-5} \quad (18)$$

where v_p is a dimensionless factor and ω is the volumetric flow.

3. Results and discussion

3.1. Effects of variables on capacity loss rate

The optimization process was performed in two steps. Based on the literature survey, a full 2^3 factorial design was carried out to identify the effect of selected variables (j, c_{act} and ω) on CL_{rate}. The combinations between these independent variables resulted in eight experiments. Table 2 describes these simulated conditions and results.

Table 2: Parameters and response of the 2^3 factorial design.

Exp	j (mA cm^{-2})	c_{act} (mol L^{-1})	ω (L min^{-1})	CL_{rate} (% $cycle^{-1}$)
1	50	1.10	15	0.59
2	100	1.10	15	0.50
3	50	1.80	15	0.87
4	100	1.80	15	0.63
5	50	1.10	30	0.57
6	100	1.10	30	0.46
7	50	1.80	30	0.86
8	100	1.80	30	0.61

The normal probability plot, shown in Figure 2.A, indicates the magnitude, direction, and importance of the effects. The effects are shown relative to a distribution fit line and negligible effects are normally distributed with mean zero on the x-axis. The significant effects have non-zero means and are further away from the red straight line.

Since the data set from the multi-physical model are unreplicated, the Lenth method [30] was used to evaluate the statistical significance of effects estimates. Lenth's pseudo standard error (PSE) is based on the concept of sparse effects and is employed to determine two critical values: marginal error (ME) and simultaneous marginal error (SME). Figure 2.B was applied to ranked variables' significance and shows the influence of the variables and cross-effects between them in the CL_{rate}. Effects with an absolute value exceeding the lines (ME and SME) are labeled statistically significant. The Pareto plot (Figure 2.B) shows that the c_{act}, j, and the interaction effect between these two variables are the most relevant parameters.

The positive estimated effect c_{act} revealed that the CL_{rate} increased with increasing c_{act} at the studied levels. That can be explained based on additive adsorption diffusional flux across the membrane due to a higher concentration gradient in the membrane/electrode interface when a larger c_{act} is applied.

Figure 3 shows integrated net fluxes (diffusional, migrational and convective) of vanadium species in the membrane/electrode interface for experiments 1, 2 and 3 from Table 2. As can be observed, diffusional flux increases for the four vanadium species when the concentration of active species goes from 1.1 to 1.8 mol L^{-1}. In contrast, the net migration and convective fluxes vary slightly for these cases. The net convective and migration fluxes are close to zero because they change direction depending on the charging or discharging procedure. The higher diffusional flux for 1.8 mol L^{-1} accelerates the variation of the VO_2^+

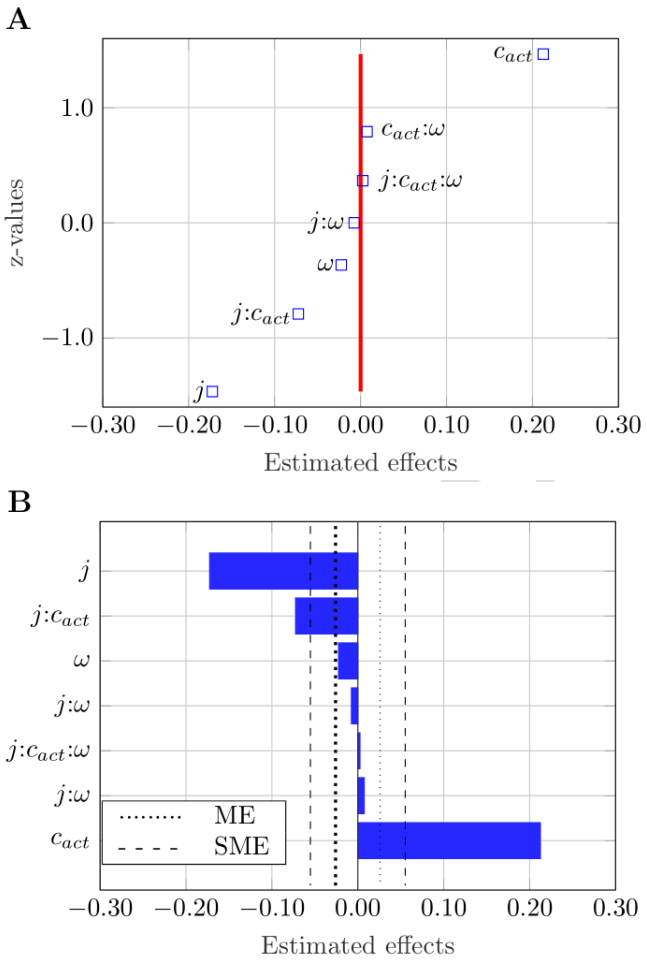

Figure 2: Normal probability plot of the effects (A) and Pareto chart (B) of the chosen variables, with the significance lines: marginal error (ME) and the simultaneous marginal error (SME).

limiting concentration during discharge, leading to higher capacity loss. Thus, the increase of c_{act} increases the diffusional fluxes across the membrane and accelerates the consumption of the limiting active species, which contributes to the self-discharge process.

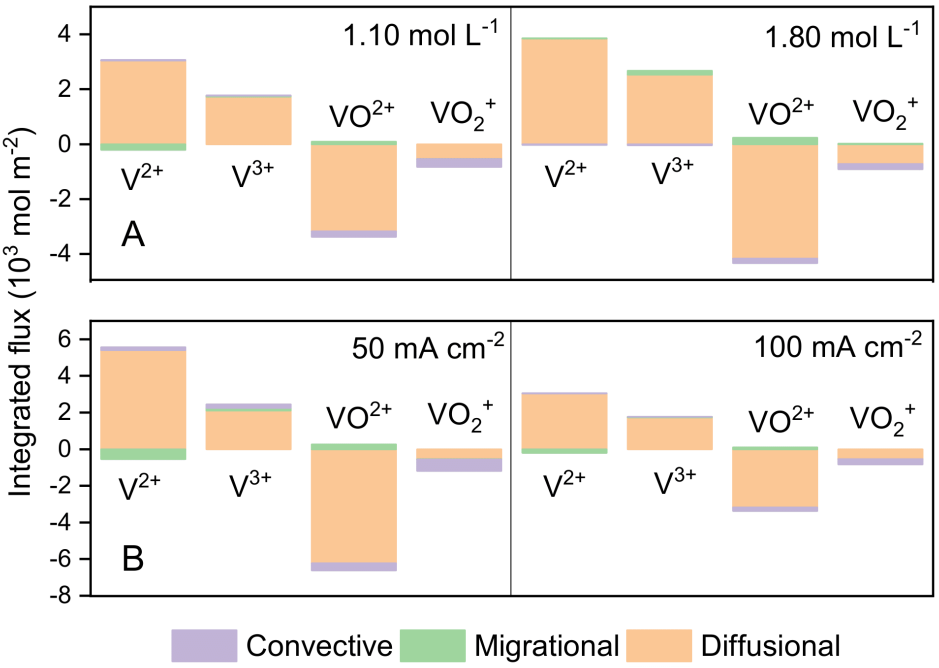

Figure 3: Comparison of integrated net fluxes across the membrane/electrolyte interface between different factorial design experiments. A: compares two levels of c_{act}, experiments 1 and 3, keeping j at 50 mA cm^{-2} and ω at 15 L min^{-1}. B: compares two levels of j, experiments 1 and 2, keeping c_{act} at 1.10 mol L^{-1} and ω at 15 L min^{-1}.

The current density has also shown a significant effect on the system, however, providing a decrease in the CL_{rate} when it is increased. Despite larger currents increasing the concentration and potential gradients in the membrane/electrolyte interface, these cases also correspond to shorter charge-discharge cycles. Thus, the integrated flux over time across the interface is smaller when larger j is used. As smaller currents lead to smaller integrated fluxes, the decrease of limiting concentration per cycle is smaller too, explaining why the CL_{rate} decreased. Thus, the increase of current density shortens the charge/discharge cycles, making fewer species cross the membrane and decreasing the capacity loss per cycle. As a consequence, the capacity loss across the cycles decreases. The interaction between c_{act} and j is also statistically significant, which is never considered when optimization is conducted by the univariate traditional mode.

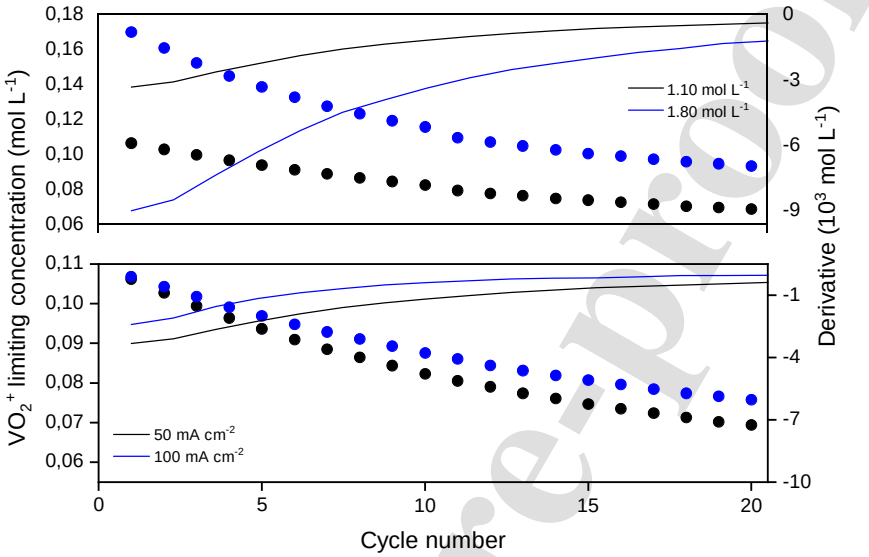

Figure 4: VO_2^+ limiting concentration during battery discharge for different values of c_{act} and j

Due to the higher diffusional flow to 1.8 mol L^{-1}, there is an acceleration in the variation of the VO_2^+ concentration limiting the concentration during the discharge. Therefore, there is a greater loss of capacity as can be seen in Figure 4. In the case of current density, the different integrated fluxes lead to different limiting concentration profiles. Since lower current densities cause lower integrated fluxes, the decrease in limiting concentration per cycle will also be smaller. Thus, there is a decrease in the capacity loss rate.

3.2. Mitigation strategy

After determining which variables affect the loss of capacity, the mitigation strategy can be applied. The strategy consists of a volume transfer between the electrolyte reservoirs in the inverse direction of net cross-contamination. This strategy is suitable due to the following self-discharge reactions that occur in the negative half-cell:

$$VO^{2+} + V^{2+} + 2H^{+} \rightarrow 2V^{3+} + H_2O \quad (19)$$

$$VO_2^{+} + 2V^{2+} + 4H^{+} \rightarrow 3V^{3+} + 2H_2O \quad (20)$$

The VO^{2+} and VO_2^{2+} species react with V^{2+} (in excess in the negative half-cell) yielding V^{3+}. Then, there is a rebalancing of V^{3+} in the negative half-cell, especially by the consumption of VO^{2+}. Therefore, this strategy may be able to partially or totally mitigate the loss of capacity.

3.2.1. Optimizing the flow velocity between reservoirs

As we saw in the previous sections the active species concentrations and the current density affect the capacity loss in a VRFB cell. We also observed that there is a region of optimum flow velocity between electrolyte reservoirs for a proper operating situation. The purpose now is to turn our general strategy by finding the optimal velocity between tanks for any condition of concentration and current. In this sense, the Doehlert design can be used to find the optimum velocity between reservoirs for any condition of current and concentration of active species. In this case of a three-variable design, fifteen combinations of parameters are tested including three replicates at the center points were carried out as shown in Table 3. As concerns the simulated space investigated, the domain of each variable was chosen according to preliminary results.

The Doehlert design is particularly appropriate in this application because it involves fewer experiments and we can move the analysis through the simulated domain with different levels for each variable [31]. This design is well-suited for constructing a second-order polynomial model and exploring quadratic response surfaces. In the present case, j, ω_{br}, and c_{act} were the variables chosen and studied in seven, five, and three values, respectively. Based on the simulated

Table 3: Three-factor Doehlert design with the corresponding responses.

Experiment	ω_{br} (µL min^{-1})	j (mA cm^{-2})	c_{act} (mol L^{-1})	CL (%)
1	1.10	80.00	1.45	0.0
2	2.00	80.00	1.45	19.4
3	1.55	114.64	1.45	4.6
4	0.20	80.00	1.45	16.3
5	0.65	45.36	1.45	2.1
6	1.55	45.36	1.45	9.2
7	0.65	114.64	1.45	7.2
8	1.55	91.56	1.78	5.8
9	0.65	68.44	1.12	4.8
10	1.55	68.44	1.12	7.7
11	1.10	103.08	1.12	2.6
12	0.65	91.56	1.78	5.5
13	1.10	56.92	1.78	0.2
14	1.10	80.00	1.70	0.2
15	1.10	80.00	1.21	1.4

data for capacity loss, a second-order equation was fitted to the prediction and can be written and decoded as

$$\begin{aligned}\mathbf{CL} = {} & 48.513 - 35.403\omega_{\mathbf{br}} - 0.0489\mathbf{j} - 37.266\mathbf{c_{act}} \\ & -0.15509\omega_{\mathbf{br}}\mathbf{:j} + 1.049\omega_{\mathbf{br}}\mathbf{:c_{act}} + 0.44230\mathbf{j:c_{act}} \\ & +21.914\omega_{\mathbf{br}}^{\mathbf{2}} + 0.001\mathbf{j^2} + 1.0570\mathbf{c_{act}^2}\end{aligned} \quad (21)$$

In equation 21 the coeficients with positive values indicate that these terms affect in favor of the response, i.e. CL. However, the terms with negative coeficients show incompatibility with CL. Analysis of variance (ANOVA) was carried out to justify the significance and adequacy of the regression model fit. The output summary statistical significance of the model was established at p = 0.05. The coeficient of determination value (R^2 of 0.998) close to unity and smaller standard deviation values indicated that the model can satisfactorily explain the data variability. The F-value of 265.6 indicates that the model is

highly adequate and meaningful. These results suggest that this model can explain 99% of the variability in the response (i.e., C_L) and only 1% of the variability is due to the noise. The relationship between the predicted data from the model and the actual data for C_L is presented in the supporting information. Specifically, data points where the actual C_L values are close to the predicted C_L values are shown. Based on the low discrepancies shown in Figure S4, it is evident that the data points are situated very close to the diagonal line. This observation, coupled with the linear arrangement of points on the graph, leads to the inference that the residuals are distributed normally.

The polynomial equation was expressed in the form of a three-dimensional surface plot which was obtained by varying two independent variables while keeping the other parameters at the static condition. Figure 5 shows the surface plots for capacity loss of ω_{br} versus j for three values of c_{act} (constant in each facet), where the minimum point is located inside the simulated region.

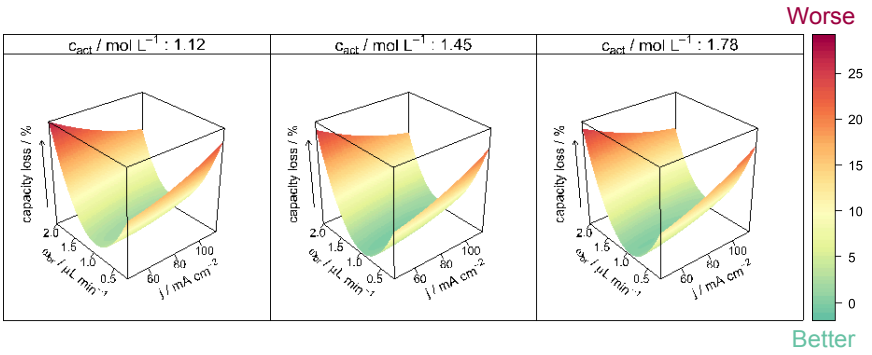

Figure 5: Capacity loss as a function of c_{act}, j and ω_{br}

It is seen that the ω_{br} has a strong non-linear influence and that the variation in C_L shows a minimum along the ω_{br} axis. The curvature in the other direction is feeble and presumably not so significant. Therefore the effect of ω_{br} and j is

not strictly linear since the equation contains both negative individual effects (first-order term) and positive quadratic coefficients. As the results show, CL will be directly decreased by j and parabolic decreased by ω_{br}. The analysis shows that the negative interaction coefficient of ω_{br}:j suggests an antagonist influence of both variables on the CL. The positive interaction coefficients ω_{br}:c_{act} and j:c_{act} suggest a synergistic influence of both variables on the CL.

By analyzing Figure 5, it is possible to verify that the surface shape can be described as an elongated saddle, and in this case, to improve the response, the directions in which the response surface decreases should be explored, so the best condition will be found on the valley. When a valley area occurs, like in Figure 5, the optimum condition will not be a single point. So when ω_{br} is between 0.75 and 1.25 µL min^{-1}, there is a local minimum for the VRFBs capacity loss when c_{act} is 1.12 mol L^{-1}. However, when c_{act} is 1.45 and 1.78 mol L^{-1} there is a global minimum for capacity loss.

Therefore, not all combinations of j and c_{act} will minimize capacity loss, but there are several minimum regions in Figure 5. Thus, it is possible to identify the optimum ω_{br} for any combination between j and c_{act} by simply choosing its values and searching for a region of minimum capacity loss. However, the surface analysis shows that although the electric current density and the concentration of active species influence the loss of capacity, the optimal volumetric flow between the reservoirs is very close to a range of variable values.

4. Conclusions

The concentration of active species and current density are the most important variables that affect capacity loss in VRFBs. Therefore, an efficient mitigation strategy based on the volume transfer between reservoirs in the reverse direction of net cross-contamination was proposed and evaluated with FEM

simulations and chemometric analysis. The proposed strategy could provide several operation conditions with different values for j and c_{act} that minimize VRFBs capacity loss. In addition, the serpentine design flow could be employed in future developments of this work for a more accurate description of mass transport. [32, 33] Thus, this study provides a set of fundamental backgrounds for experimental work bringing an understanding of the effects of operating conditions on the performance of VRFBs.

5. Acknowledgments

The support of this research by FAPESP grant: 2013/07296-2, 2017/11986-5, 2019/11095-9, 2019/27029-5, 2021/03592-2, 2021/11630-1, 2022/05254-0, Shell, CNPq and CAPES (Code 001).

References

[1] I. E. Agency, World energy outlook 2022, https://www.iea.org/reports/world-energy-outlook-2021, 2021.

[2] T. M. Gür, Review of electrical energy storage technologies, materials and systems: challenges and prospects for large-scale grid storage, Energy & Environmental Science 11 (2018) 2696–2767. URL: https://pubs.rsc.org/en/content/articlehtml/2018/ee/c8ee01419ahttps://pubs.rsc.org/en/content/articlelanding/2018/ee/c8ee01419a. doi:10.1039/C8EE01419A.

[3] R. Chen, S. Kim, Z. Chang, R. Chen, S. Kim, Z. Chang, Redox flow batteries: Fundamentals and applications, Redox - Principles and Advanced Applications (2017). URL: https://www.intechopen.com/chapters/55442undefined/chapters/55442. doi:10.5772/INTECHOPEN.68752.

[4] D. Azhgaliyeva, Energy Storage and Renewable Energy Deployment: Empirical Evidence from OECD countries, Energy Procedia 158 (2019) 3647–3651. URL: https://linkinghub.elsevier.com/retrieve/pii/S1876610219309415. doi:10.1016/j.egypro.2019.01.897.

[5] A. Z. Weber, M. M. Mench, J. P. Meyers, P. N. Ross, J. T. Gostick, Q. Liu, Redox flow batteries: A review, Journal of Applied Electrochemistry 41 (2011) 1137–1164. URL: https://link.springer.com/article/10.1007/s10800-011-0348-2. doi:10.1007/S10800-011-0348-2/FIGURES/15.

[6] Y. Shi, C. Eze, B. Xiong, W. He, H. Zhang, T. M. Lim, A. Ukil, J. Zhao, Recent development of membrane for vanadium redox flow battery applications: A review, Applied Energy 238 (2019) 202–224. doi:10.1016/J.APENERGY.2018.12.087.

[7] W. Wang, Q. Luo, B. Li, X. Wei, L. Li, Z. Yang, Recent Progress in Redox Flow Battery Research and Development, Advanced Functional Materials 23 (2013) 970–986. URL: https://onlinelibrary.wiley.com/doi/full/10.1002/adfm.201200694https://onlinelibrary.wiley.com/doi/abs/10.1002/adfm.201200694https://onlinelibrary.wiley.com/doi/10.1002/adfm.201200694. doi:10.1002/ADFM.201200694.

[8] P. Leung, A. Shah, L. Sanz, C. Flox, J. Morante, Q. Xu, M. Mohamed, C. Ponce de León, F. Walsh, Recent developments in organic redox flow batteries: A critical review, Journal of Power Sources 360 (2017) 243–283. URL: https://linkinghub.elsevier.com/retrieve/pii/S0378775317306985. doi:10.1016/j.jpowsour.2017.05.057.

[9] S. Wang, K. A. Owusu, L. Mai, Y. Ke, Y. Zhou, P. Hu, S. Magdassi, Y. Long, Vanadium dioxide for energy conservation and energy storage

applications: Synthesis and performance improvement, Applied Energy 211 (2018) 200–217. doi:10.1016/J.APENERGY.2017.11.039.

[10] Nagmani, D. Pahari, P. Verma, S. Puravankara, Are Na-ion batteries nearing the energy storage tipping point? – Current status of non-aqueous, aqueous, and solid-sate Na-ion battery technologies for sustainable energy storage, J. Energy Storage 56 (2022) 105961. doi:10.1016/j.est.2022.105961.

[11] A. Khor, P. Leung, M. R. Mohamed, C. Flox, Q. Xu, L. An, R. G. Wills, J. R. Morante, A. A. Shah, Review of zinc-based hybrid flow batteries: From fundamentals to applications, Materials Today Energy 8 (2018) 80–108. doi:10.1016/J.MTENER.2017.12.012.

[12] P. Leung, X. Li, C. Ponce De León, L. Berlouis, C. T. Low, F. C. Walsh, Progress in redox flow batteries, remaining challenges and their applications in energy storage, RSC Advances 2 (2012) 10125–10156. URL: https://pubs.rsc.org/en/content/articlehtml/2012/ra/c2ra21342ghttps://pubs.rsc.org/en/content/articlelanding/2012/ra/c2ra21342g. doi:10.1039/C2RA21342G.

[13] Y. Wang, P. He, H. Zhou, Li-Redox Flow Batteries Based on Hybrid Electrolytes: At the Cross Road between Li-ion and Redox Flow Batteries, Advanced Energy Materials 2 (2012) 770–779. URL: https://onlinelibrary.wiley.com/doi/full/10.1002/aenm.201200100https://onlinelibrary.wiley.com/doi/abs/10.1002/aenm.201200100https://onlinelibrary.wiley.com/doi/10.1002/aenm.201200100. doi:10.1002/AENM.201200100.

[14] D. Pletcher, R. Wills, A novel flow battery: A lead acid battery based on an electrolyte with soluble lead(II), Physical

Chemistry Chemical Physics 6 (2004) 1779–1785. URL: https://pubs.rsc.org/en/content/articlehtml/2004/cp/b401116chttps://pubs.rsc.org/en/content/articlelanding/2004/cp/b401116c. doi:10.1039/B401116C.

[15] J. Cheng, L. Zhang, Y. S. Yang, Y. H. Wen, G. P. Cao, X. D. Wang, Preliminary study of single flow zinc–nickel battery, Electrochemistry Communications 9 (2007) 2639–2642. doi:10.1016/J.ELECOM.2007.08.016.

[16] P. K. Leung, C. Ponce De León, F. C. Walsh, An undivided zinc–cerium redox flow battery operating at room temperature (295 K), Electrochemistry Communications 13 (2011) 770–773. doi:10.1016/J.ELECOM.2011.04.011.

[17] C. Zhang, L. Zhang, Y. Ding, S. Peng, X. Guo, Y. Zhao, G. He, G. Yu, Progress and prospects of next-generation redox flow batteries, Energy Storage Materials 15 (2018) 324–350. doi:10.1016/J.ENSM.2018.06.008.

[18] Y. Lu, J. B. Goodenough, Rechargeable alkali-ion cathode-flow battery, Journal of Materials Chemistry 21 (2011) 10113–10117. URL: https://pubs.rsc.org/en/content/articlehtml/2011/jm/c0jm04222fhttps://pubs.rsc.org/en/content/articlelanding/2011/jm/c0jm04222f. doi:10.1039/C0JM04222F.

[19] Y. Lu, J. B. Goodenough, Y. Kim, Aqueous cathode for next-generation alkali-ion batteries, Journal of the American Chemical Society 133 (2011) 5756–5759. URL: https://pubs.acs.org/doi/full/10.1021/ja201118f. doi:10.1021/JA201118F/SUPPL_FILE/JA201118F_SI_001.PDF.

[20] Y. Zhao, Y. Ding, Y. Li, L. Peng, H. R. Byon, J. B. Goodenough, G. Yu, A chemistry and material perspective on lithium

redox flow batteries towards high-density electrical energy storage, Chemical Society Reviews 44 (2015) 7968–7996. URL: https://pubs.rsc.org/en/content/articlehtml/2015/cs/c5cs00289chttps://pubs.rsc.org/en/content/articlelanding/2015/cs/c5cs00289c. doi:10.1039/C5CS00289C.

[21] R. F. Gahn, N. H. Hagedorn, J. S. Ling, SINGLE CELL PERFORMANCE STUDIES ON THE Fe/Cr REDOX ENERGY STORAGE SYSTEM USING MIXED REACTANT SOLUTIONS AT ELEVATED TEMPERATURE., NASA Technical Memorandum (1983). URL: https://www.osti.gov/servlets/purl/6005325/. doi:10.2172/6005325.

[22] M. Skyllas-Kazacos, M. Rychick, R. Robins, All-vanadium redox battery, 1988.

[23] Vanadis power – changing energy storage, URL: https://www.vanadispower.com/.

[24] K. E. Rodby, T. J. Carney, Y. Ashraf Gandomi, J. L. Barton, R. M. Darling, F. R. Brushett, Assessing the levelized cost of vanadium redox flow batteries with capacity fade and rebalancing, J. Power Sources 460 (2020) 227958. doi:10.1016/j.jpowsour.2020.227958.

[25] K. Wang, L. Liu, J. Xi, Z. Wu, X. Qiu, Reduction of capacity decay in vanadium flow batteries by an electrolyte-reflow method, J. Power Sources 338 (2017) 17–25. doi:10.1016/j.jpowsour.2016.11.031.

[26] D. C. Montgomery, Design and Analysis of Experiments, 8 ed., John Wiley & Sons, Nashville, TN, 2012.

[27] V. Czitrom, One-factor-at-a-time versus designed experiments, The Ameri-

can Statistician 53 (1999) 126. URL: https://doi.org/10.2307/2685731. doi:10.2307/2685731.

[28] M. Esteban, M. Ariño-Blasco, J. Díaz-Cruz, Chemometrics in electrochemistry, in: Comprehensive Chemometrics, Elsevier, 2020, pp. 1–31. URL: https://doi.org/10.1016/b978-0-12-409547-2.14622-0. doi:10.1016/b978-0-12-409547-2.14622-0.

[29] G. Wosiak, M. C. Silva, J. da Silva, E. B. Carneiro-Neto, M. C. Lopes, E. Pereira, Evaluation of interfacial pH change during water splitting at pulsed regime using finite element method, Int. J. Hydrogen Energy 46 (2021) 17644–17652. doi:10.1016/j.ijhydene.2021.02.195.

[30] R. V. Lenth, Quick and easy analysis of unreplicated factorials, Technometrics 31 (1989) 469–473. URL: http://www.jstor.org/stable/1269997.

[31] C. R. T. Tarley, G. Silveira, W. N. L. dos Santos, G. D. Matos, E. G. P. da Silva, M. A. Bezerra, M. Miró, S. L. C. Ferreira, Chemometric tools in electroanalytical chemistry: Methods for optimization based on factorial design and response surface methodology, Microchemical Journal 92 (2009) 58–67. URL: https://www.sciencedirect.com/science/article/pii/S0026265X09000186. doi:https://doi.org/10.1016/j.microc.2009.02.002, polar Chemistry.

[32] E. Ali, H. Kwon, J. Kim, H. Park, Numerical study on serpentine design flow channel configurations for vanadium redox flow batteries, Journal of Energy Storage 32 (2020) 101802. doi:10.1016/J.EST.2020.101802.

[33] Q. He, J. Yu, Z. Guo, J. Sun, S. Zhao, T. Zhao, M. Ni, Modeling of vanadium redox flow battery and electrode optimization with different flow fields, e-Prime - Advances in Electrical Engineering, Electronics and Energy 1 (2021) 100001. doi:10.1016/J.PRIME.2021.100001.

Highlights

Mitigating the capacity loss by crossover transport in vanadium redox flow battery: A chemometric efficient strategy proposed using finite element method simulation

Luis F. Pilonetto, Felipe Staciaki, Eryka Nóbrega, Evaldo B. Carneiro-Neto, Jeyse da Silva, Ernesto Pereira

- Computational approach to mitigate the VRFB capacity loss by cross-contamination.
- Current density and active species concentration majorly impact VRFB capacity loss.
- Mitigation strategy reduces VRFB capacity loss across diverse operational conditions.

Mitigating the capacity loss by crossover transport in vanadium redox flow battery: A chemometric efficient strategy proposed using finite element method simulation

Luis F. Pilonetto[1], Felipe Staciaki[1], Eryka Nóbrega[1], Evaldo B. Carneiro-Neto[1], Jeyse da Silva[1], Ernesto Pereira[1,]

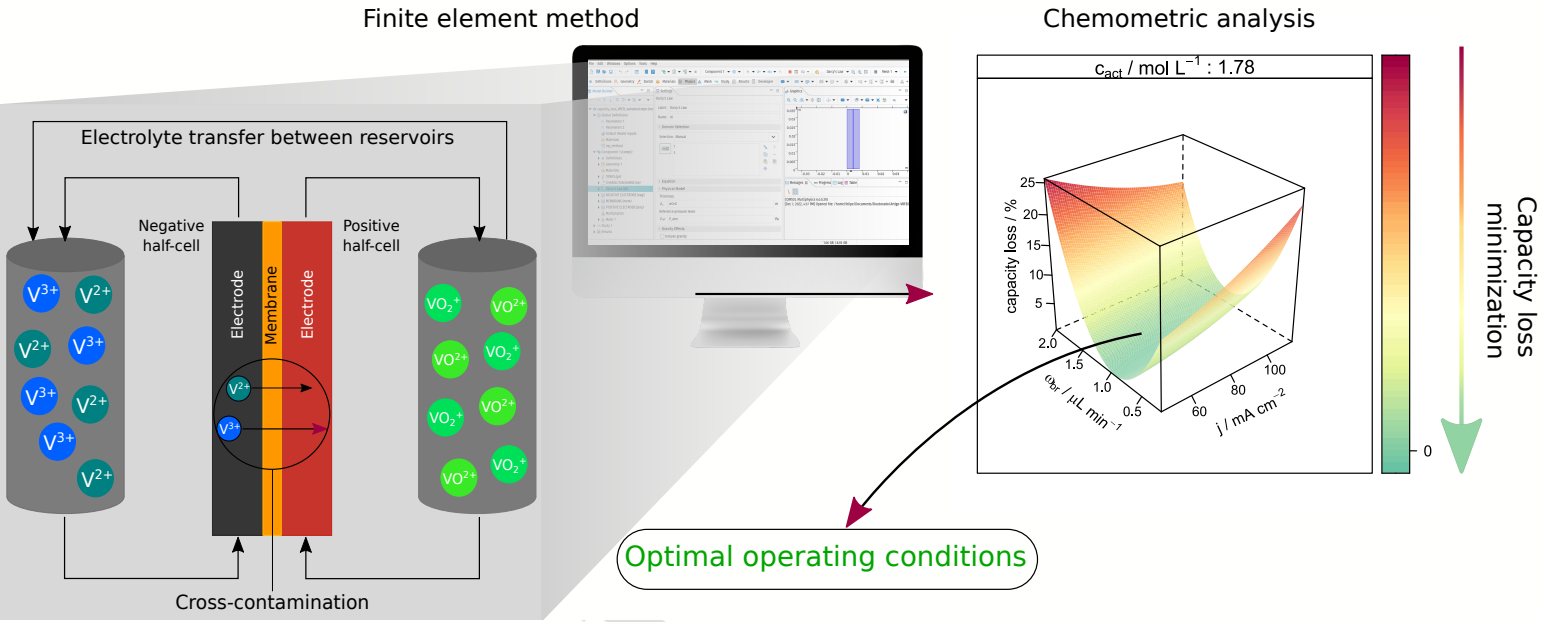

Declaration of interests

☒ The authors declare that they have no known competing financial interests or personal relationships that could have appeared to influence the work reported in this paper.

☐ The authors declare the following financial interests/personal relationships which may be considered as potential competing interests: